We are IntechOpen, the world's leading publisher of Open Access books Built by scientists, for scientists

4,800
Open access books available

122,000
International authors and editors

135M
Downloads

Our authors are among the

154
Countries delivered to

TOP 1%
most cited scientists

12.2%
Contributors from top 500 universities

CLARIVATE ANALYTICS BOOK CITATION INDEX INDEXED

WEB OF SCIENCE™

Selection of our books indexed in the Book Citation Index in Web of Science™ Core Collection (BKCI)

Interested in publishing with us?
Contact book.department@intechopen.com

Numbers displayed above are based on latest data collected.
For more information visit www.intechopen.com

23

Foamed Nanocomposites for EMI Shielding Applications

Isabel Molenberg, Isabelle Huynen, Anne-Christine Baudouin, Christian Bailly, Jean-Michel Thomassin and Christophe Detrembleur
Université Catholique de Louvain, Université de Liège
Belgium

1. Introduction

The addition of nanoparticles having specific properties inside a matrix with different properties creates a novel material that exhibits hybrid and even new properties. The nanocomposites presented in this paper combine the properties of foamed polymers (inexpensive, lightweight, easy to mould into any desired shape, etc.) with those of carbon nanotubes (CNTs). The addition of any conductive nanoparticles to an otherwise insulating matrix leads to a significant increase of the electrical conductivity. But CNTs have a very high aspect ratio; a much lower content of CNTs is therefore required to get the same conductivity increase as the one obtained with more compact nanoparticles.
This is especially interesting for EMI shielding materials since, as will be explained in further details in this chapter, it is desirable for such materials to have a high conductivity but a low dielectric constant, in order to minimize the electromagnetic power outside the shield casing but also to minimize the power reflected back inside the casing, as is explained in section 2. In particular, two parameters of interest when comparing shielding materials are detailed and discussed.
The polymer/CNTs nanocomposites were fabricated and characterized using a two-step diagnostic method. They were first characterized in their solid form, i.e. before the foaming process and the most interesting polymer matrices (with embedded CNTs) could be selected. This way, only the promising blends were foamed, therefore avoiding the unnecessary fabrication of a number of foams. These selected blends were foamed and then characterized. The samples, both solid and foamed, are described and their fabrication processes are briefly explained in section 3 while the characterization methods are shown in section 4.
A simple electrical model is given and explained in section 5 and an optimized topology for the foams is also proposed in the second part of the same section.
The measurement results for the solids and for the mono-layered and multi-layered foams are summarized and discussed in section 6. They are then compared to results obtained using the electrical model presented in the previous section and they are also correlated to rheological characterizations.

2. EMI shielding considerations

There are two main parameters that are used to characterize the quality of a shielding material in terms of electromagnetic power; the Shielding Effectiveness (SE) and the Reflectivity (R). The former relates the power that is transmitted through the material (P_{out}), cf. Fig. 1(left), to the incident power (P_{in}): SE = 10 log (P_{in}/P_{out}). The latter relates the power reflected back from the material (P_{ref}) to the incident power (P_{in}): R=10 log(P_{ref}/P_{in}).
The incident power is either reflected back, or transmitted through the material to the outer world, or absorbed inside the material, $P_{in} = P_{ref} + P_{out} + A^2$, where A^2 is the power absorbed inside the material. A is called the attenuation and increases as the conductivity of the material increases. The power reflected at the interface air-material is higher when the difference between the dielectric constants on both sides of the interface is more important. Since air has a dielectric constant of 1, the Reflectivity increases with the dielectric constant of the shielding material.
It must be noted that the above discussion does not take into account the reflection at the second interface, material to air. To be exact we should consider this extra reflection but its effect becomes negligible when the attenuation is sufficiently high, cf. (Huynen et al., 2008).
It is not always enough for a shielding material to exhibit a good SE, i.e. stopping power transmission to the outside world. For example, metallic materials have a high SE at high frequency but almost all the incident power is reflected back inside the shield casing (high R), possibly interfering with other inner elements (or even with the emitter itself). Materials that combine a high SE with a low R at microwave frequencies are called microwave absorbers, because the power is absorbed inside the material, cf. Fig. 1(right). For a material to have a high SE, it must exhibit a high conductivity and, in order to have a low R, it must have a low dielectric constant.

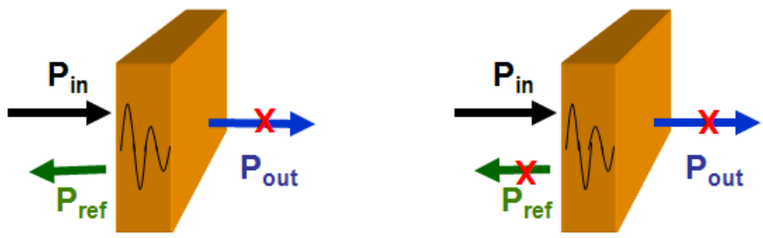

Fig. 1. Schematic diagrams for a conventional metallic shielding material (left) and for a microwave absorber (right).

Finding a material that combines a high electrical conductivity and a low dielectric constant is not trivial. This is the idea behind the use of foamed nanocomposites. In theory, foaming a material would decrease its dielectric constant (because of the porosity and because air has dielectric constant of 1). On the other hand, the addition of conductive nanoparticles to a material should theoretically increase its conductivity, cf. (Huynen et al., 2008), (Thomassin et al., 2008).
Besides having a potentially low dielectric constant, polymer foams are inexpensive, lightweight and easy to mould into any desirable shape. And, the addition of conductive nanoparticles would also reinforce the polymer matrix, improving its electrical conductivity but also its mechanical properties and its thermal conductivity, cf. (Saib et al. 2006). Carbon

nanotubes have a very high aspect-ratio (≥1000). They can therefore form extensive regular conductive networks with a much lower content than other nanoparticles having a more spherical or compact shape, cf. Fig. 2.

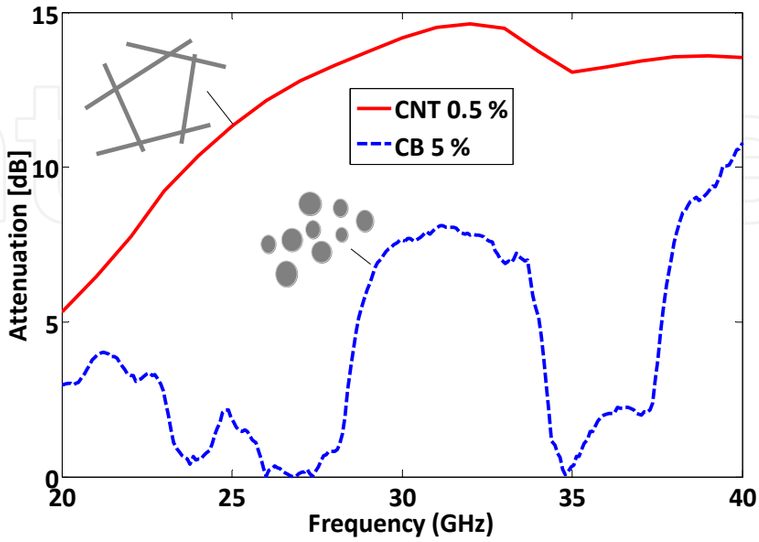

Fig. 2. Influence of the type of nanoparticles, CBs or CNTs, on the attenuation of a nanocomposite, from (Saib et al. 2006).

The applications of such foamed nanocomposites are numerous and varied, from electronics packaging to bioneural matrices, in aeronautics, automotive, environmental applications, and many more...
But the most promising application at the moment is certainly as shielding materials, more precisely as microwave absorbers. They could be made into thin, large, flexible, lightweight panels to be used as EMI shielding materials anywhere, and for little cost. Those panels could also have interesting fire retardancy or protection again electrostatic discharges properties.

3. Nanocomposite samples description

The chemical processes involved in the fabrication of foamed samples are rather complex, cf. section 3.2 for more details. It is therefore interesting to make a first selection on the nanocomposite blends before they are actually foamed. A two-step diagnostic method was developed; solid samples of polymer-CNTs blends were first characterized (the so-called screening tests), the best candidate blends were then used to fabricate foams and finally the foamed samples were also characterized.

3.1 Solid thin-film samples (screening tests)

The CNTs used for the fabrication of the nanocomposites are commercially available thin MultiWalled NanoTubes (MWNTs), with an average outer diameter of 10 nm and a purity over 95%. They were produced using Catalytic Carbon Vapour Deposition (CCVD) by Nanocyl SA (Belgium).

The polymer/CNTs composites were fabricated using two different techniques, cf. (Thomassin et al., 2008). The first one consists in melt-blending the polymer matrix, poly(ε-caprolactone) (PCL), with CNTs using a DSM microextruder. The second one, called the "coprecipitation" technique, is the solubilization of PCL in an organic solvent (tetrahydrofurane, THF, especially well suited to PCL) in the presence of the required amount of CNTs. After 30 seconds of ultrasonic treatment in order to break the CNTs bundles, the mixture is poured into heptane, which is a poor solvent for PCL. The polymer then instantly precipitates and the CNTs are trapped in it.
At this stage the samples are in solid form, cf. FIG. 3, they have not yet been foamed, they are simply referred to as "solid samples" throughout the chapter.

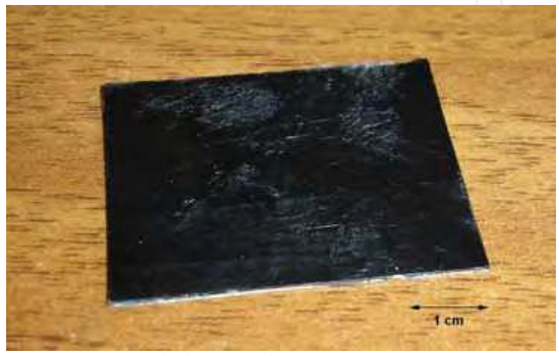

Fig. 3. Picture of a nanocomposite solid sample.

3.2 Foamed samples

Solid samples prepared by the methods described in the previous section were foamed using supercritical CO_2. They were first pressurized at about 200 bars at 60°C for 3h in order to saturate the sample with CO_2. The pressure was then rapidly released in a few seconds leading to the foaming of the sample. A picture of a foamed nanocomposite fabricated this way is shown on FIG. 4 (already cut into pieces prior to its characterization), cf. (Thomassin et al., 2008)

Fig. 4. Picture of a nanocomposite foamed sample (already cut into pieces prior to its characterization).

4. Characterization methods

A two-step diagnostic method to find the polymer-CNTs nanocomposites best fitted for shielding applications was developed, cf. (Molenberg et al., 2009); solid samples of polymer-CNTs blends were first characterized using a microstrip one-line method, cf. section 4.2, the best candidates were used to fabricate foams that were then characterized using a waveguide line-line method, cf. section 4.1.
Even if different methods were used to characterize the various samples, they were all based on the measurement of their scattering parameters (S_{ii}) using a Vector Network Analyzer (VNA). The dielectric constant and conductivity of the samples were then extracted from these parameters. Those measurements were made in the 8-40 GHz frequency band.
The foams were measured using waveguides, while the solid samples were measured using microstrips. This is due to their respective geometries, thin flat solid samples would not fill the waveguides enough to make precise measurements while foams are too porous and thick to be reliably measured in a microstrip configuration.

4.1 Line-line waveguide configuration technique

The Line-Line (LL) method is based on the extraction of the propagation constant (γ), cf. FIG. 5, from the measurement of the scattering parameters (S_{ij}) of two transmission lines of different lengths, here two waveguides having their inner volumes entirely filled with the sample under test, cf. (Huynen et al., 2001), (Saib et al., 2006) and (Pozar, 2005).

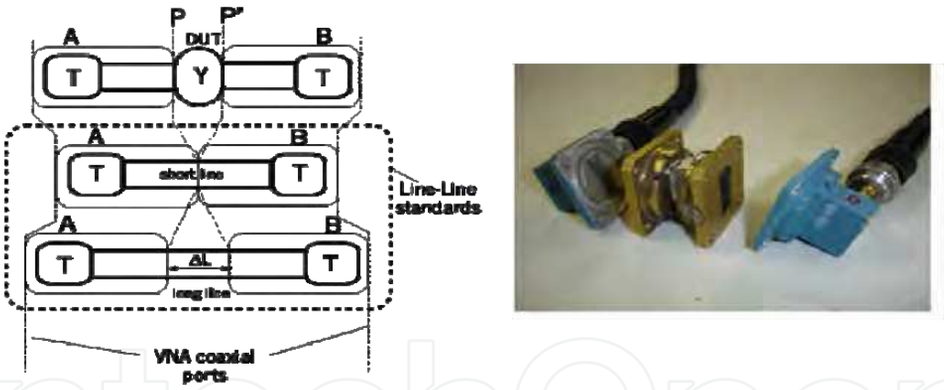

Fig. 5. Line-line method, from (Huynen et al., 2001) and experimental set-up for the Line-Line method, waveguide, transitions and coaxial cables to the VNA.

From the scattering parameters of both lines, their transfer matrices T_{L1} and T_{L2} can be extracted. After a few mathematical operations, a matrix $T_{\Delta L}$ can be calculated. It is diagonal and has the form

$$T_{\Delta L} = \begin{pmatrix} e^{-\gamma \Delta L} & 0 \\ 0 & e^{-\gamma \Delta L} \end{pmatrix} \quad (1)$$

And from the propagation constant, the dielectric constant and conductivity can be easily determined

$$\varepsilon_r = \varepsilon^{'} - j\varepsilon^{''} = \left(\frac{c_0\gamma}{j\omega}\right)^2 \text{ and } \sigma = -\omega\varepsilon_0\varepsilon^{''} \tag{2}$$

It should be noted that the magnitude of diagonal element $e^{-\gamma\Delta L}$ in equation (1) corresponds to the attenuation undergone by the signal over a thickness ΔL of material. As γ is proportional to σ, it further confirms that a high conductivity is required for obtaining a good absorption.

Only a simple coaxial SOLT (short-return-through-line) calibration of the VNA is required and the final values of permittivity and conductivity depend only on the length difference ΔL. It is therefore especially well suited to waveguide measurements, because there is no precision waveguide calkit available in our laboratory. Such a calkit would have been necessary for more complex and accurate calibrations. The comparison between the simple SOLT calibration method and a LRM (Line-Reflect-Match) method, a more precise technique using a reference calkit, is illustrated on Fig. 6. With an LRM calibration, the reference planes of the VNA are brought after the coaxial-microstrip transitions, so that the VNA measures the scattering parameters of the line under test only. With a SOLT calibration, the VNA reference planes are placed before these transitions and their influence on the measurements of each line is not eliminated. Nevertheless, the SOLT calibration is sufficient to make sure that the $T_{\Delta L}$ matrix is diagonal, therefore ensuring the validity of the LL method.

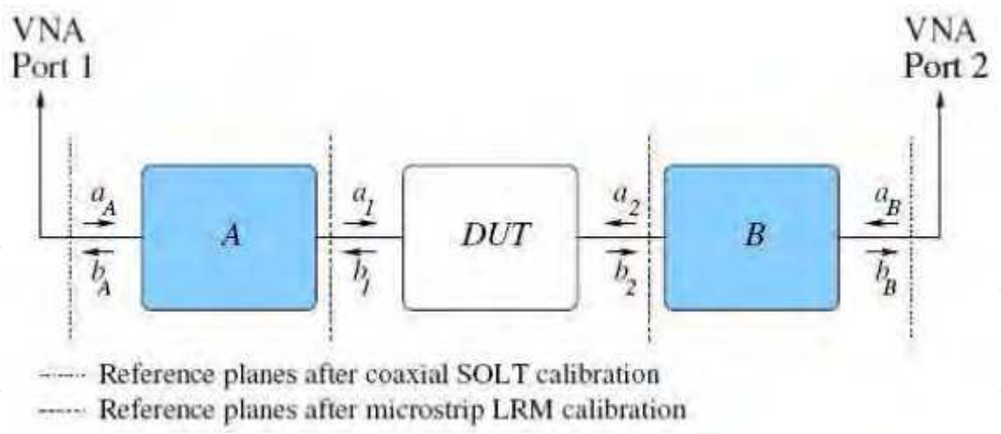

Fig. 6. Schematics of the measurement setup where A and B correspond to the coaxial-to-microstrip transition, and DUT to the device-under-test, from (Saib et al., 2004).

4.2 One-line characterization in microstrip configuration technique

The One-Line method is based on the measurement of the scattering parameters (S_{ii}) of only one line (different from the LL method described in the previous section), a microstrip line in this case. The sample to be characterized is used as substrate to fabricate a microstrip transmission line. A thin copper ribbon is glued to the top of the sample, serving as microstrip and a piece of aluminum tape is glued on the bottom of the solid sample, to form

the ground plane, cf. Fig. 7(right). From the S matrix, the ABCD chain matrices can be calculated for a transmission line of length L and of characteristic impedance Z_c, cf. (Saib, 2004)

$$ABCD = \begin{pmatrix} ch(\gamma L) & Z_C sh(\gamma L) \\ \frac{1}{Z_C} sh(\gamma L) & ch(\gamma L) \end{pmatrix} \quad (3)$$

The propagation constant γ can then be extracted and the dielectric constant and conductivity can be determined, using equation (2).
This method is valid only if a precise LRM calibration of the VNA has been done. The reference planes must be put after the transitions, and the reference impedances in these planes must be set to 50 Ω, which is ensured using an LRM calibration. An Anritsu precision microstrip calkit and the corresponding 3680K Anritsu sample holder (including the transitions) were used for the microstrip measurements, cf. Fig. 7.

Fig. 7. Experimental set-up for the One-Line method applied to a microstrip topology, entire set-up (left), Anritsu sample holder (right) with the microstrip visible on top of the sample (substrate).

5. Modelling, design and optimization

5.1 Simple electrical model

It must first be noted that Carbon Black (CB) nanoparticles, i.e. relatively spherical carbon platelets, are considered here instead of CNTs to simplify geometrical considerations.
As can be seen on conductivity-versus-frequency plots resulting from nanocomposites measurements, cf. section 6 and (Saib et al., 2006), the measured conductivity tends to 0 for very low frequencies. This means that the conductive nanoparticles do not form a direct conductive pathway for the electrons from one side of the sample to the other side. However, at relatively high frequency the conductivity becomes significant, indicating the presence of capacitive couplings between the nanoparticles. Taking these observations into

account, a simple electrical model was developed, cf. (Saib et al., 2006). This model is represented on Fig. 8. The nanocomposite is placed between a ground plane and a microstrip line, to form a microstrip transmission line, the actual configuration of the (solid) samples during the measurements, cf. section 5.2 and 6.1.

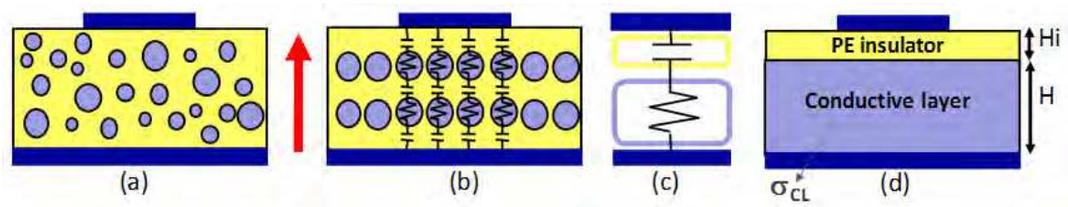

Fig. 8. Simple electrical model explaining the frequency dependence of the conductivity of the nanocomposites, from (Saib et al., 2006): (a) first approximation, the CB nanoparticles are spherical, well dispersed inside the polymer matrix and not in physical contact with one another. The arrow indicates the dominant direction of the electric field. (b) Second approximation, the CB particles form a regular network of conductive grains inside an insulating polymer matrix. (c) Equivalent admittance per unit length of microstrip line. (d) Corresponding two-layer microstrip transmission line.

The CB nanoparticles are supposed to be spherical and well dispersed inside the matrix. There is also supposed to be no direct physical contact between them, i.e. they do not touch one another, cf. Fig. 8(a). This random distribution is approximated by a regular homogeneous network of purely conductive grains inside a completely insulating polymer matrix. Therefore, the electrical equivalent of each grain is a simple resistor and there are strong capacitive couplings between all the grains. Since the electric field distribution between the top and bottom conductors of the microstrip line is quasi uniform and perpendicular to those conductors, only capacitors and resistors that are parallel to that direction have to be considered, cf. Fig. 8(b). This corresponds to a two-layered microstrip transmission line, cf. Fig. 8(d), with an insulating top layer and a conductive bottom layer (conductivity = σ_{CL}). This line has an electrical equivalent admittance per unit length that corresponds to a simple resistor-capacitor (R_T and C_T) series circuit, cf. Fig. 8(c). The simulated results obtained using this simple model are confronted with measurement results in section 6.3.

5.2 Optimization of the topology of the samples

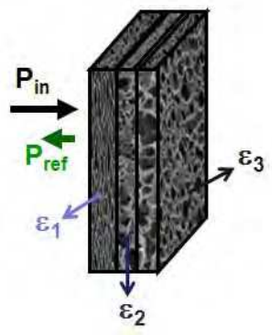

Fig. 9. Schematic diagram the three-layered foam, with $\varepsilon_1 < \varepsilon_2 < \varepsilon_3$.

In order to improve the reflectivity of the shielding material, it would be interesting to create a foam having a gradient of dielectric constant inside the material, analogous to the stealth paint protecting some spy aircrafts from radar detection. A way to achieve this gradient is to fabricate multilayered foams, each layer having a different, increasing dielectric constant, cf. Fig. 9.
The measurement results for a three-layered nanocomposite fabricated as previously described are shown and discussed in section 6.4.

6. Results and discussion

6.1 Solid samples

Microstrip transmission lines were fabricated, using the nanocomposite thin films as substrates. By connecting these lines to a 2-port vector network analyzer (VNA), their scattering parameters were measured and the dielectric constant and conductivity of the samples were then extracted, using the One-Line method described in section 4.2.
The results presented in this section were obtained for composites based on different polymer materials: PS (polystyrene), PCL (poly(ε-caprolactone)), PVC (polyvinyl chloride) and PMMA (polymethyl methacrylate), they all had a 2% CNT content. As can be seen on Fig. 10 and Fig. 11, the PMMA-based sample exhibited the lowest dielectric constant but not highest conductivity, while the PCL-based composite had the highest conductivity but also the highest dielectric constant.

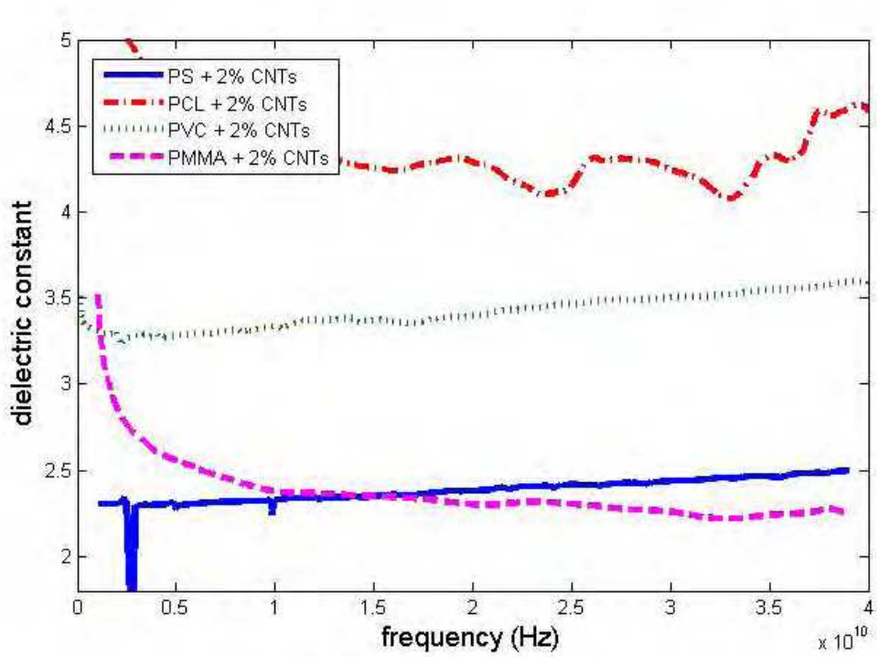

Fig. 10. Measured dielectric constant of four solid nanocomposite samples versus frequency (composites based on different polymer matrices).

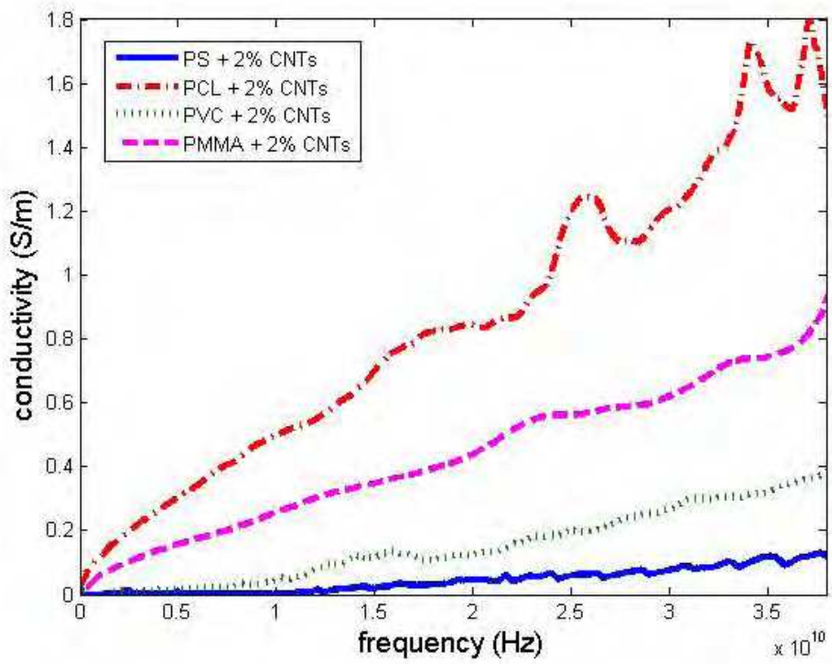

Fig. 11. Measured conductivity of the solid nanocomposite samples versus frequency (composites based on different polymer matrices).

Once a polymer matrix is selected, an optimal content of CNTs to add into the matrix must be determined. It can be shown that the addition of CNTs increases the conductivity of the nanocomposite but also increases its dielectric constant, which is not desired. Since foamed samples have lower dielectric constants than solid ones with the same composition, the exact content of CNTs should be chosen after measurement of foamed samples rather than solid ones, cf. section 6.2.
It should also be noted that other chemical process parameters have a non-negligible influence. Those are beyond the scope of the present chapter, but can be found in (Thomassin et al., 2007).

6.2 Foamed samples

PCL was selected as polymer matrix because it exhibited the highest conductivity in its solid form, cf. Fig. 11. Its dielectric constant was also the highest one, cf. Fig. 10, but foaming the nanocomposite should significantly decrease it. The foamed samples were inserted in four waveguides of different dimensions, covering the 8 to 40 GHz band, cf. Fig. 5. Their scattering parameters were measured using the Line-Line method described in section 4.1.
As mentioned in the previous section, a foamed material has a lower dielectric constant than a solid one of the same chemical composition. This is shown on Fig. 12, the black and red curves correspond to PCL samples with no CNT content, and the dielectric constant of the solid sample is twice that of the foam. It can be explained by the porosity of the foams and the subsequent presence of air inside the sample, the air having a dielectric constant of 1.

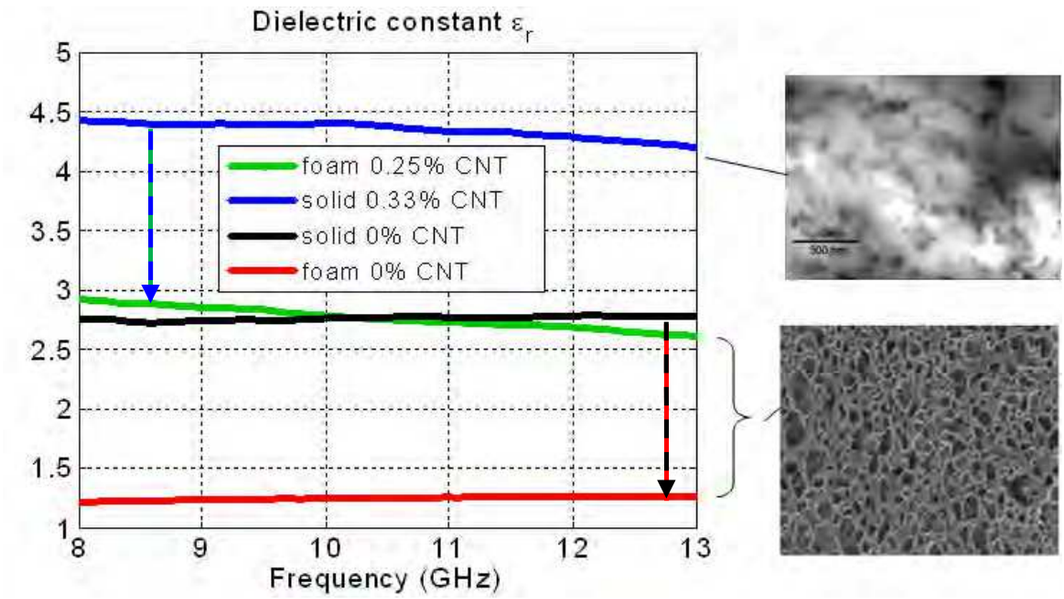

Fig. 12. Measured dielectric constant of solid and foamed PCL nanocomposite samples, all having a similar CNT content.

On the other hand, the conductivity of foams is usually higher than that of solid samples, mainly because the CNT are forced into the side walls of pores in the foamed material and this way form a more regular network. This effect is shown on Fig. 13 for a foam and a solid sample having a close but not equal CNT content, both PCL composites.

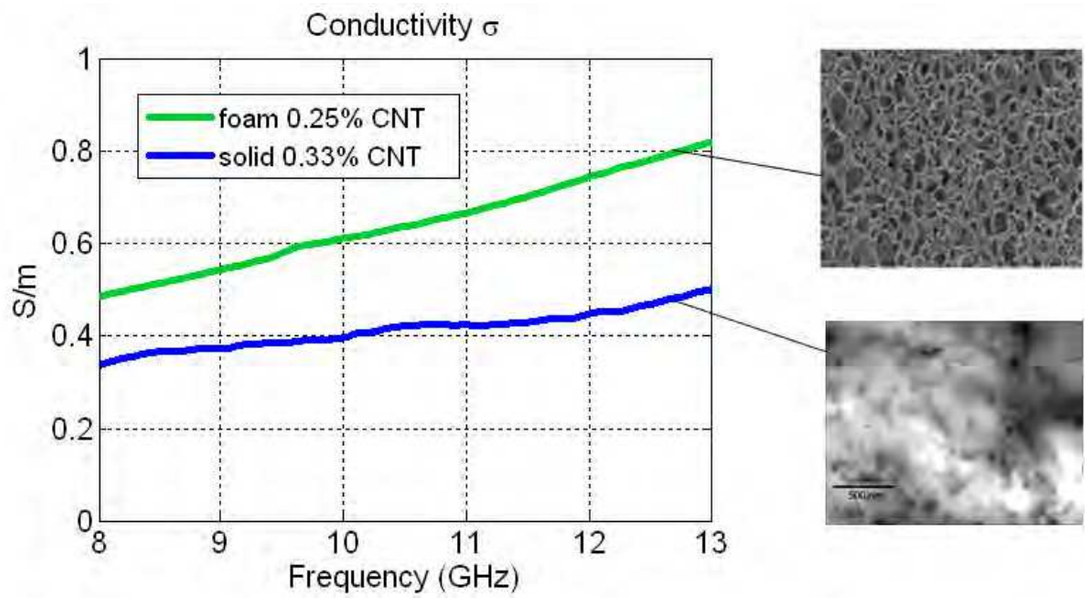

Fig. 13. Measured conductivity of solid and foamed PCL/CNTs nanocomposite samples, both having a similar CNT content.

The conductivity of foamed nanocomposites increases significantly with the CNT content, as can be seen on Fig. 14(left) and the Shielding Effectiveness also increases in the same proportions, cf. Fig. 14(right). Therefore, in order to have a good SE, it appears, from these results, that the CNT content must be as high as possible.

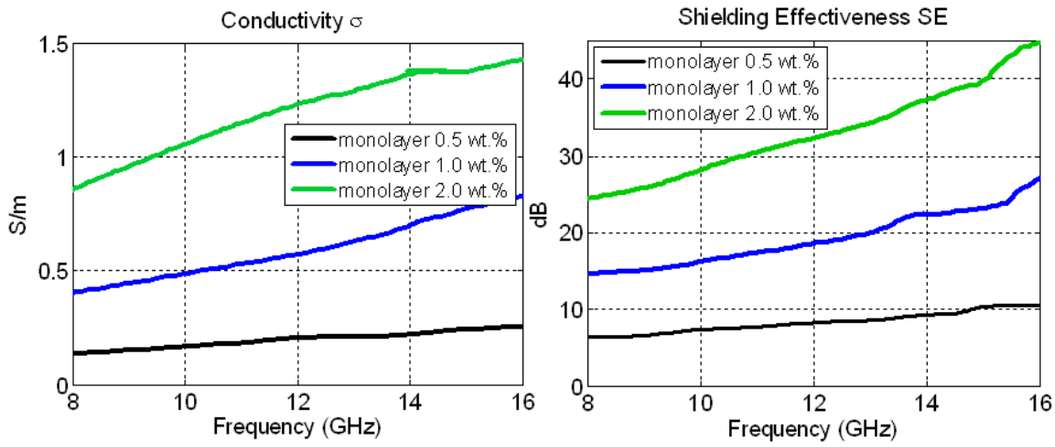

Fig. 14. Measured conductivity of foamed PCL nanocomposite samples with increasing CNT contents (left) and the corresponding Shielding Effectiveness (right).

But the addition of CNTs has an adverse effect on the Reflectivity because the dielectric constant increases significantly with CNT content, cf. Fig. 15. To measure R, a metallic sheet (or Perfect Electrical Conductor – PEC) is added on the output interface, cf. Fig. 9, and the sample with the PEC sheet is then characterized (Line-line method, same as samples without PEC). Part of the incident power is absorbed inside the material, the remaining power then reaches the PEC where it is totally reflected and, another part of the power is absorbed on the way back. Because of the PEC, the SE in this configuration is theoretically infinite. The power reflected back to the port 1 of the VNA, cf. Fig. 6, is the combination of the power directly reflected back at the input interface and the power reaching the metallic plate and being reflected back (the remaining power that has not been absorbed by the material on the way back).

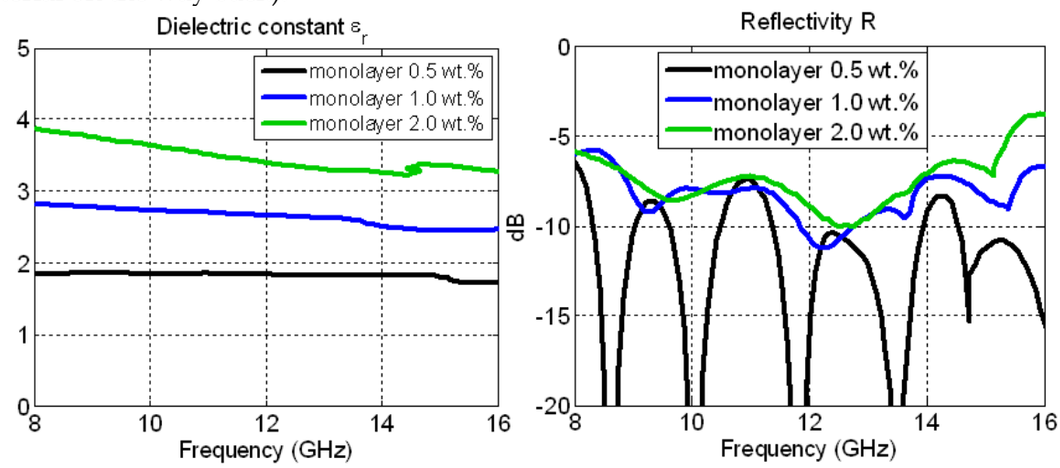

Fig. 15. Measured dielectric constant of foamed PCL nanocomposite samples with increasing CNT contents (left) and the corresponding Reflectivity (right).

In conclusion, foamed nanocomposites have both a higher conductivity and a lower dielectric constant than solid samples. The first are therefore better suited for shielding applications than the latter. The optimum CNT content has to be the result of a compromise between Shielding Effectiveness and Reflectivity, i.e. between conductivity and dielectric constant.

6.3 Comparison between results using the electrical model and from measurements

According to the electrical model developed in section 5.1, at low frequency, since there are no physical contacts between the grains, the equivalent capacitor, cf. Fig. 8(c), is a virtual 'open-circuit'; therefore there is no current flowing through the composite. At high enough frequency, the equivalent capacitor is a virtual short circuit and the conductivity becomes constant. Its value depends then only on the conductivity of the conductive layer of Fig. 8(d). In other words, at low frequency when $(\omega C_T)^{-1} >> R_T$, the conductivity is very low. At high frequency, when $(\omega C_T)^{-1} << R_T$, the conductivity is constant. In between, the conductivity increases with frequency. This corresponds to a transition frequency, f_T, equal to $f_T = (2\pi R_T C_T)^{-1}$.

The dielectric constant and conductivity extracted using this model and the values from measurements are plotted on Fig. 16 and Fig. 17 for CNT contents of 50% and 0.35 %, respectively. The conductivity of the conductive bottom layer (σ_{CL}) was arbitrarily chosen to be equal to 25 S/m. The height of the top layer (H_i) was adjusted in order to obtain the best fit between model and measurement results.

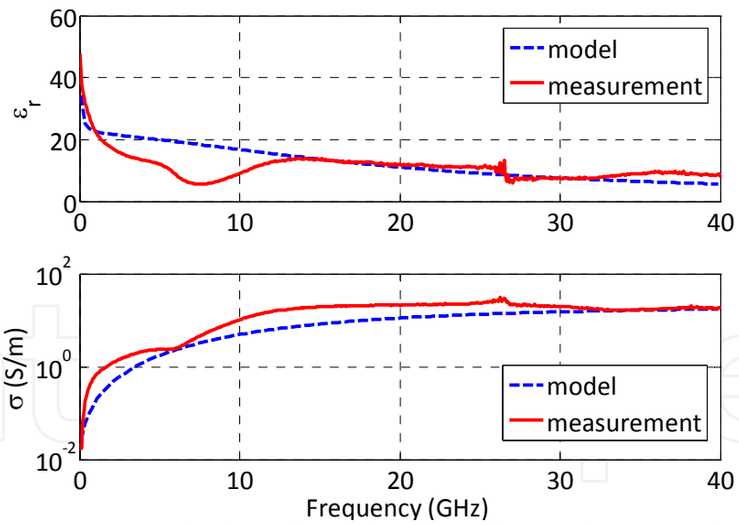

Fig. 16. Dielectric constant (top) and conductivity (bottom) extracted using the simple electrical model and from actual measurements, for a CNT content of 50% (model parameters: $H/H_i = 93/7$ with $H + H_i = 0.8$ mm and $\sigma_{CL} = 25$ S/m), from (Saib et al., 2006).

As can be seen on Fig. 16(bottom), the results obtained using our model and those from measurements show a very good adequacy. At low frequency the conductivity tends to zero. At high frequency there is a plateau, i.e. a constant conductivity. The transition

frequency is of about 10 GHz. At this frequency, a behaviour change can also be observed in the dielectric constant-versus-frequency plot, cf. Fig. 16(top).
A CNT (weight) content of 50% is very high. The conductivity and dielectric constant were simulated and measured for a much more realistic CNT content of 0.35%. The results are shown on Fig. 17, the saturation plateau in the conductivity-versus-frequency plot is not reached at 40 GHz but it is expected that with a CNT content as low as 0.35%, the transition frequency would be well over 100 GHz. Nevertheless, the results obtained using the electrical and those from measurements are still in very good adequacy. It must be noted that the H/H_i ratio is very different for the 0.35 and 50% CNT content models. It can be easily understood considering that the average distance between the conductive particles decreases as the concentration of these particles is increased.

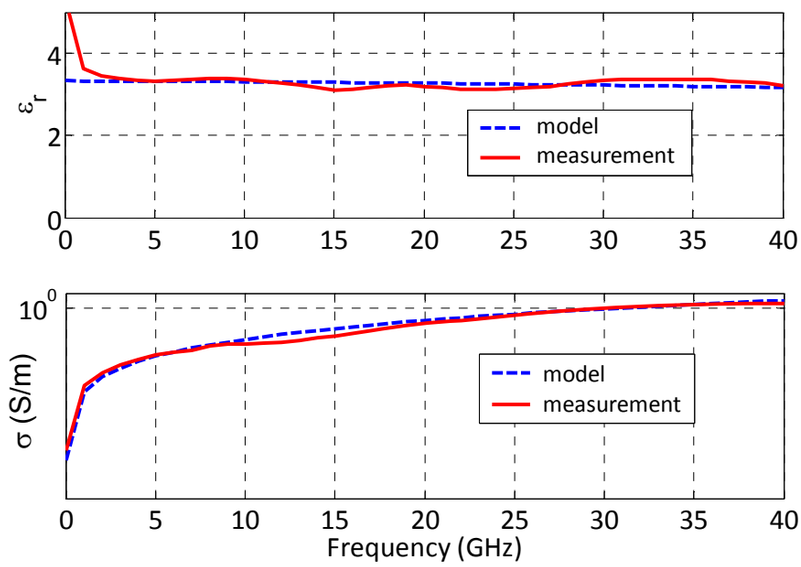

Fig. 17. Dielectric constant (top) and conductivity (bottom) extracted using the simple electrical model and from actual measurements, for a CNT content of 0.35% (model parameters: $H/H_i = 40/60$ with $H + H_i = 0.8$ mm and $\sigma_{CL} = 25$ S/m), from (Saib et al., 2006).

In conclusion, the simple electrical model developed in section 5.1 for CB particles can explain and fit very well the frequency dependence of the conductivity and dielectric constant of polymer/CNTs nanocomposites. The model shows that different frequency behaviours of nanocomposites are related to different CNT contents, or different volumetric H/H_i ratios in the model, hence different mean distances between particles.

6.3 Correlation between the electrical and rheological characterizations

As explained in sections 5.1 and 6.3, a good dispersion of the CNTs inside the polymer matrix is the key parameter for the conductivity of the nanocomposites. The mean distance between two CNTs should also be as small as possible. But raw CNTs, before they are incorporated in the polymer matrix, are entangled and tend to stick to one another, as confirmed by the Transmission Electron Microscope (TEM) picture shown on Fig. 18.

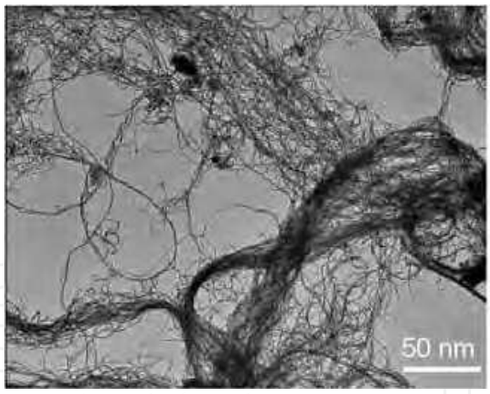

Fig. 18. TEM picture of raw MWNT before they are incoporated into the polymer matrix, from (Saib et al., 2006).

Rheological measurements can also be used to assess the dispersion of the CNTs, in particular the (oscillatory) frequency dependence of the dynamical complex modulus G*, which is the ratio of stress to strain when a sinusoidal stress or strain is applied to the sample (Dynamical Mechanical Analysis or DMA), cf. (Saib et al., 2006). For elastic materials, G* is real; the response to the sinusoidal strain is also sinusoidal and in-phase with the stimulus. For visco-elastic materials like the polymer presented in this paper, G* is complex; the response is also sinusoidal but with a phase shift. The real part (G') of the dynamical modulus is the in-phase, elastic, response of the material, while the imaginary part (G'') is the out-of-phase, viscous response. In polymers such as PCL or PS, an increase of G' with CNT content at low frequency confirms the presence of mobile and flexible chains that are partially bound together by bridging structures, here the CNTs.
The real part of G* is plotted versus frequency for two sets of PS and PCL based nanocomposites, with and without CNTs, on FIG. 19. The presence of saturation at low frequency for the PCL samples containing CNTs is characteristic of the existence of a percolation threshold, after which the CNTs form a network throughout the polymer matrix, cf. Fig. 19(left).
On the contrary, there is little difference between the G'-versus-frequency curve for the PS sample with 1% CNTs and the one for pure PS, cf. Fig. 19(right). It means that the nanoparticles do not form an extended network inside the PS matrix.

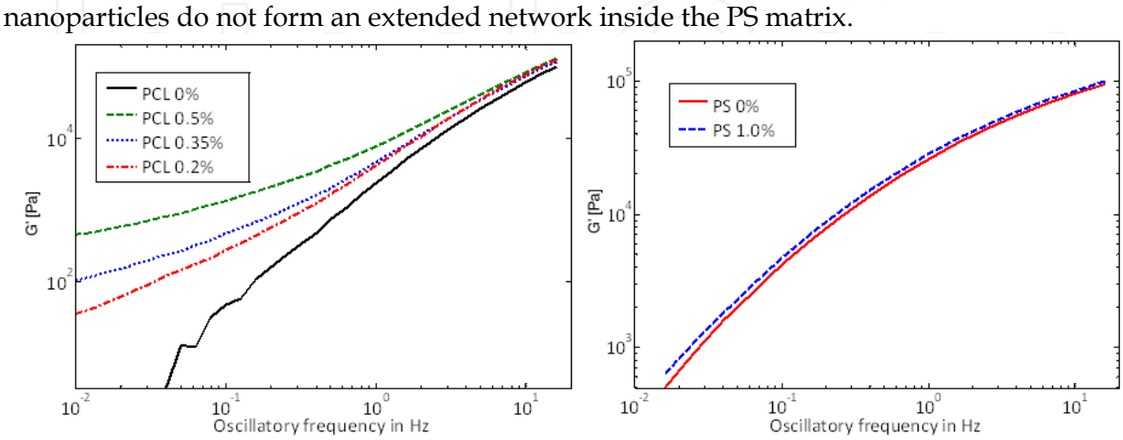

Fig. 19. Dynamical modulus real part (G') versus frequency for PCL and PS based nanocomposites, with and without CNTs, from (Saib et al., 2006).

These conclusions based upon rheological considerations are confirmed by the measurement of the electrical conductivity. The conductivities of the PCL nanocomposite with a 0.35% CNT content and of the PS one with a concentration of 1% are plotted versus frequency on Fig. 20. The electrical model explained how the value of the electrical conductivity was linked to the mean distance between the particles and therefore to the presence of a regular, well-dispersed nanoparticles network, cf. (Saib et al., 2006). The PCL composite has a much higher conductivity than the PS one, confirming the presence of a conductive network in the former and not in the latter. This is further confirmed by TEM pictures, cf. Fig 21. The CNTs in the PCL sample seem well dispersed forming an extensive network while those in the PS composite are regrouped in distinct aggregates, over 1µm apart.

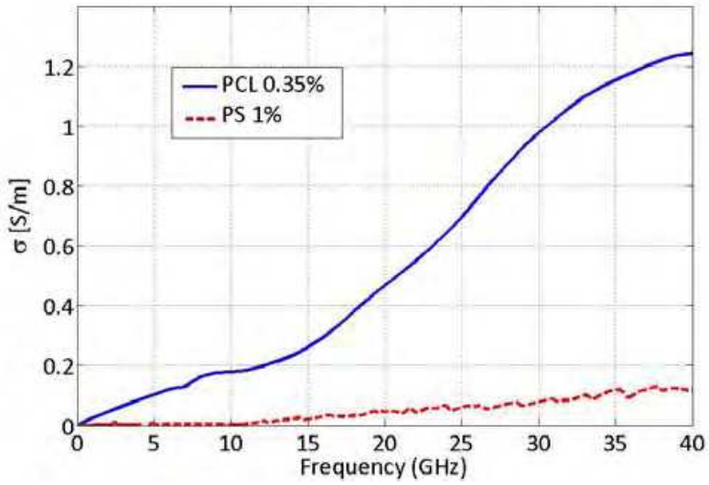

Fig. 20. Measured electrical conductivity versus frequency of the PCL composite containing a 0.35% CNT content and of the PS sample with a 1% CNT content, from (Saib et al., 2006).

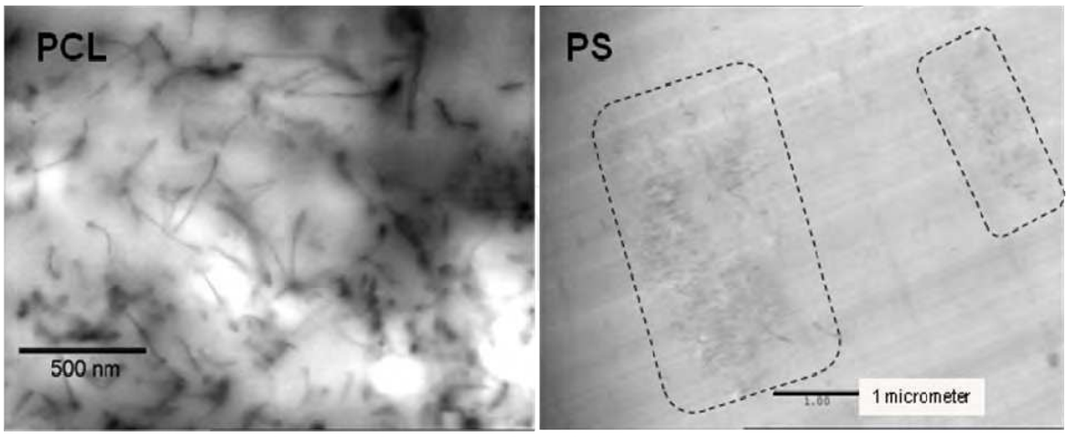

Fig. 21. TEM pictures of the PCL (left) and PS (right) nanocomposites.

6.4 Optimized multilayered foamed samples

As explained in section 5.2, a multilayered foam sample with graded concentrations of CNTs should exhibit simultaneously a high Shielding Effectiveness with a low dielectric constant for a lower CNT content.

A multilayered foam consisting of three layers of PCL with graded CNT contents (0.5%, 1% and 2% for layers 1.2, 1.1 and 0.7 cm thick, respectively) was fabricated and characterized. The total thickness of the sample is therefore equal to 3 cm and the average CNT concentration is equal to 1.03%.
The conductivity and dielectric constant were measured between 8 and 16 GHz. The Shielding Effectiveness and Reflectivity were then extracted. The results are shown on Fig. 22, along with the results for the mono-layered samples of section 6.2. As can be seen on this figure, the multi-layered foam has the same SE as the mono-layered one with the same CNT concentration as the average CNT content of the multi-layered sample. But its Reflectivity is much lower than that of all the mono-layered foams!
The graded concentration achieved by the cascade of layers with increasing CNT concentration, combined with foaming, ensures a progressive and moderate increase in dielectric constant, meaning that reflection P_r at input interface of each layer is minimized, power entering the composite is maximized, and reflection is significantly reduced over a broad frequency range. The progressive increase in conductivity yielded by graded concentration contributes to the absorption of the most part of the power over the depth of the structure by conductive dissipation.

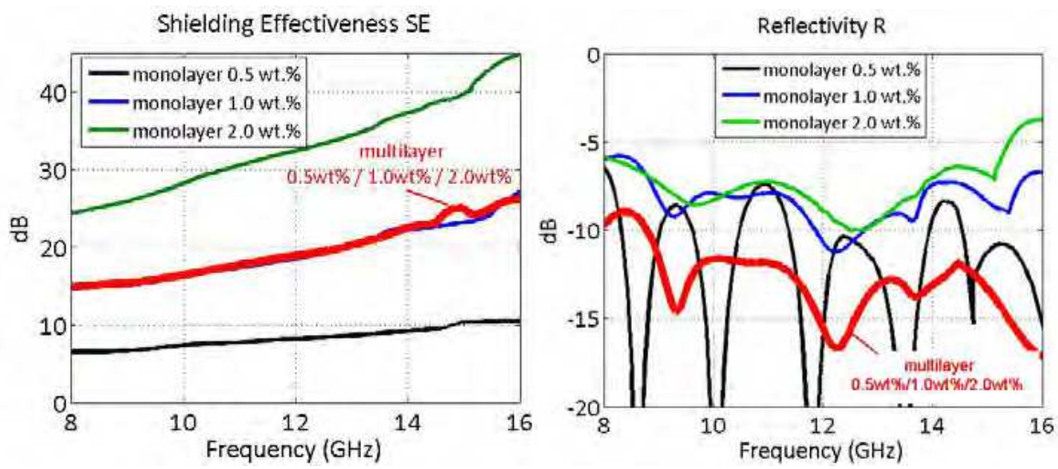

Fig. 22. Shielding Effectiveness (left) and Reflectivity (right) of the multilayered and mono-layered samples, from (Huynen et al., 2008).

The measurements therefore confirm the high potential of multilayered foams for EMI shielding applications.

7. Conclusion

Throughout this chapter, we have seen that foamed polymer/CNTs nanocomposites make very good EMI shielding materials. They exhibit a high conductivity and a relatively low dielectric constant, leading to a high Shielding Effectiveness and a relatively low Reflectivity, although a compromise in CNT content must be found between a high SE and a low R. This was confirmed by measurement results and rheological measurements but also using a simple electrical equivalent model.

Some EMI shielding considerations were first presented. In particular, the notions of SE and R were defined and the advantage of microwave absorbers on conventional metallic shielding materials was discussed. The samples were briefly described, both foamed and in their solid form, along with their fabrication methods. The electrical characterization techniques were presented and their adequacy to the samples under test was briefly discussed. An optimized multi-layered foam topology with increasing CNT contents in each subsequent layer was proposed.

The measurement results of the solid samples, mono- and multi-layered foams, were detailed and discussed. Physical explanations were proposed. These results were also compared to those obtained using the equivalent model and rheological characterization techniques, with a very good adequacy. The three-layered foam exhibited a SE similar to that of a mono-layered sample having the same average CNT content but the R of the multi-layered foam was significantly decreased.

To conclude, nanocomposite foams have good EMI properties but a compromise on the CNT content must be found in order to have a high SE and also a low R. On the other hand, multi-layered foams with graded concentrations of CNTs are especially well suited to EMI shielding applications, having a high SE with a lower R than mono-layered samples.

8. References

Huynen I., Steukers C. & Duhamel F. (2001). A wideband line-line dielectrometric method for liquids, soils, and planar substrates. *IEEE Transactions on Instrumentation and Measurement,* Vol. 50, No. 5, (October 2001) pp. 1343-1348, 0018-9456

Huynen I., Bednarz L., Thomassin J.-M., Pagnoulle C., Jerome R. & Detrembleur C. (2008). Microwave absorbers based on foamed nanocomposites with graded concentration of carbon nanotubes, *Proceedings of the 38th European Microwave Conference*, pp. 5-8, 978-2874870064, Amsterdam, April 2008, IEEE, Piscataway

Molenberg I., Thomassin J.-M., Ferain E., Detrembleur C. & Huynen I. (2009). RF Diagnostic Methods for Two Nanostructured Polymer Applications, pp. 1045-1048, 978-2874870118, Rome, *Proceedings of the 39th European Microwave Conference*, Roma, September 2009, IEEE

Pozar D. (2004). *Microwave Engineering,* Wiley, 978-0471448785, New York

Saib A. (2004). *Modeling and design of microwave devices based on ferromagnetic nanowires*. PhD Thesis, Presses Universitaires de Louvain, 978-2930344776, Louvain la Neuve

Saib A., Bednarz L., Daussin R., Bailly C., Lou X., Thomassin J.-M., Pagnoulle C., Jerome R. & Huynen I. (2006). Carbon nanotubes composites for broadband microwave absorbing materials. *IEEE Transactions on Microwave Theory and Techniques*, Vol. 54, No. 6, (June 2006) pp. 2745-2752, 0018-9480

Thomassin J.-M., Pagnoulle C., Bednarz L., Huynen I., Jerome R. & Detrembleur C. (2008). Foams of polycaprolactone/MWNT nanocomposites for efficient EMI reduction. *Journal of Materials Chemistry*. Vol. 18, No. 7, (January 2008) pp. 792-796, 0959-9428

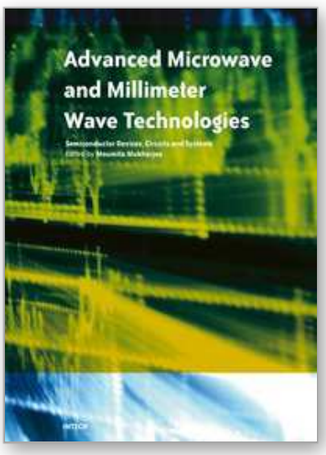

Advanced Microwave and Millimeter Wave Technologies
Semiconductor Devices Circuits and Systems
Edited by Moumita Mukherjee

ISBN 978-953-307-031-5
Hard cover, 642 pages
Publisher InTech
Published online 01, March, 2010
Published in print edition March, 2010

This book is planned to publish with an objective to provide a state-of-the-art reference book in the areas of advanced microwave, MM-Wave and THz devices, antennas and systemtechnologies for microwave communication engineers, Scientists and post-graduate students of electrical and electronics engineering, applied physicists. This reference book is a collection of 30 Chapters characterized in 3 parts: Advanced Microwave and MM-wave devices, integrated microwave and MM-wave circuits and Antennas and advanced microwave computer techniques, focusing on simulation, theories and applications. This book provides a comprehensive overview of the components and devices used in microwave and MM-Wave circuits, including microwave transmission lines, resonators, filters, ferrite devices, solid state devices, transistor oscillators and amplifiers, directional couplers, microstripeline components, microwave detectors, mixers, converters and harmonic generators, and microwave solid-state switches, phase shifters and attenuators. Several applications area also discusses here, like consumer, industrial, biomedical, and chemical applications of microwave technology. It also covers microwave instrumentation and measurement, thermodynamics, and applications in navigation and radio communication.

INTECH
open science | open minds

InTech Europe
University Campus STeP Ri
Slavka Krautzeka 83/A
51000 Rijeka, Croatia
Phone: +385 (51) 770 447
Fax: +385 (51) 686 166

InTech China
Unit 405, Office Block, Hotel Equatorial Shanghai
No.65, Yan An Road (West), Shanghai, 200040, China
中国上海市延安西路65号上海国际贵都大饭店办公楼405单元
Phone: +86-21-62489820
Fax: +86-21-62489821

IntechOpen

IntechOpen